Electronic Supplementary Information for

Supramolecular Step-Growth Polymerization Kinetics of Pre-Assembled Triblock Copolymer Micelles

Yingqing Lu,† Liang Gao,† Jiaping Lin, Liquan Wang, Liangshun Zhang* and Chunhua Cai*

Shanghai Key Laboratory of Advanced Polymeric Materials, State Key Laboratory of Bioreactor Engineering, Key Laboratory for Ultrafine Materials of Ministry of Education, School of Materials Science and Engineering, East China University of Science and Technology, Shanghai 200237, China

Contents

1 Copolymer synthesis, self-assembly and characterization

Materials

α,ω-diamino-poly(ethylene glycol) (NH_2-PEG-NH_2) (M_w=2000) was purchased from Sigma Inc. γ-benzyl-L-glutamate-*N*-carboxyanhydride (BLG-NCA) was synthesized according to literatures.[S1-S3] Deionized water was prepared in a Millipore Super-Q Plus Water System to a level of 18.2 MΩ cm resistance. Analytical grade of 1,4-dioxane was refluxed with sodium and distilled immediately before use. All the other reagents were of analytical grade and used as received. The dialysis bag (Membra-cel, 3500 molecular weight cutoff) was provided by Serva Electrophoresis GmbH.

Synthesis of PBLG-*b*-PEG-*b*-PBLG triblock copolymers

Poly(γ-benzyl-L-glutamate)-*block*-poly(ethylene glycol)-*block*-poly(γ-benzyl-L-glutamate) triblock copolymers (PBLG-*b*-PEG-*b*-PBLG) were synthesized by ring-opening polymerization of γ-benzyl-L-glutamate-N-carboxyanhydride (BLG-NCA) initiated by NH_2-PEG-NH_2 with 1,4-dioxane as solvent.[S4,S5] After reacted at room temperature for 3 days, the viscous reaction mixture was poured into a large volume of anhydrous ethanol. The precipitated product was dried under vacuum and then purified twice by repeated precipitation from a chloroform solution into a large volume of anhydrous methanol. Finally, the product was dried under vacuum and white power was collected. In this work, two kinds of copolymers denoted by $PBLG_{252}$-*b*-PEG_{45}-*b*-$PBLG_{252}$ and $PBLG_{167}$-*b*-PEG_{45}-*b*-$PBLG_{167}$ were prepared. The subscripts denote the repeating units of the blocks. Detailed information regarding the characteristics of the triblock copolymers is provided in the Section 2 in the following text.

Preparation of hierarchical 1D assemblies through a two-step self-assembly process

The preparation process of the micellar solution is represented in Scheme S1. In the first-step assembly, initial micellar subunits were prepared. The PBLG-*b*-PEG-*b*-PBLG copolymers were dissolved in THF/DMF (1/1, v/v) mixed solvents by stirring the stock solutions at room temperature for 2 days (polymer concentration of initial solution was 0.25 g/L). To prepare the initial micelle solution, deionized water was added dropwise to the PBLG-*b*-PEG-*b*-PBLG initial solution with vigorous stirring, reaching a water content of 16.7 vol%. By changing the temperature in the above processes, the structure of subunits could be adjusted. After equilibration, the initial subunits were frozen by rapidly adding a large amount of water and dialyzing the solution against water. The obtained aqueous solution of the initial subunits was concentrated with rotary evaporator to a final concentration of 0.6 g/L. For the studies of the effect of the subunit concentration on the higher-level assembly, the concentrated aqueous subunit solution was diluted into different volumes via the addition of water.

In the second-step assembly, 3.0 mL of DMF was pipetted into 3.0 mL the initial subunit solution. (The volume ratio of water/DMF in the final solution was 1/1.) The subunits were thus activated and the assembly began. To characterize the aggregate morphologies, at various experimental intervals, we pipetted 0.5 mL of sample solution into a large amount of water to freeze the morphologies. The obtained solution was dialyzed against water to remove all the organic solvents before observation. The second assembly step was conducted at the constant temperature of 30 ^{o}C. Finally, the sample was characterized by SEM and TEM.

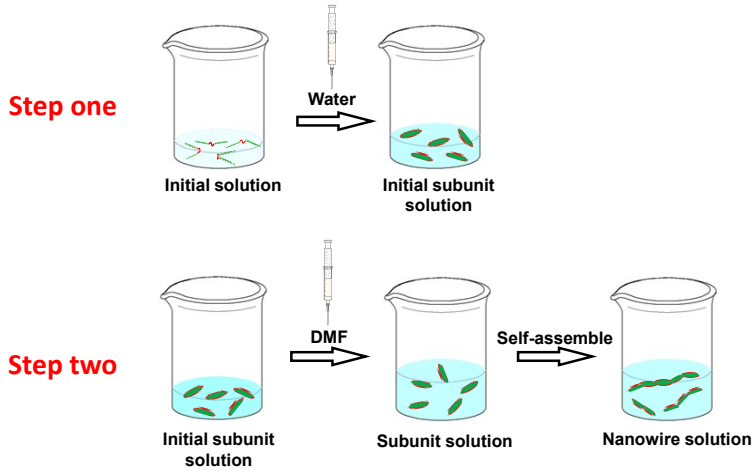

Scheme S1. Schematic representation of the step-wise self-assembly process.

Characterization

Transmission Electron Microscopy (TEM)

The morphologies of aggregates were examined by TEM (JEM-2100F, JEOL) operated at an accelerating voltage of 200 kV. The samples were prepared by placing a drop of solution on a carbon film coated copper grid and quickly freezing the solution in liquid nitrogen. The frozen samples were then dried in a vacuum.

Cryo-TEM

Cryo-TEM samples were prepared in a controlled environment vitrification system (CEVS) at 25^{o}C. One drop of sample solution was placed on a copper grid coated with carbon film. The excess solution was blotted with a piece of filter paper, and then quickly dipped into liquid ethane, which was cooled by liquid nitrogen. The vitrified samples were then stored in liquid nitrogen until they were transferred to a cryogenic sample holder (Gatan 626) and examined with JEM-2200FS TEM (200 kV) at about -174^{o}C.

Scanning Electron Microscopy (SEM)

The morphologies of aggregates were also observed by SEM (S4800, HITACHI) operated at an accelerating voltage of 15 kV. The samples were prepared by placing a drop of solution on a copper grid coated with carbon film and quickly freezing the solution in liquid nitrogen. The frozen samples were then dried in a vacuum. Before the observations, the samples were sputtered by Aurum.

Dynamic light scattering measurements (DLS)

DLS measurements were performed at a scattering angle of 90° on a commercial LLS spectrometer (ALV/CGS-5022) equipped with an ALV-High QE APD detector and an ALV-5000 digital correlator using a He-Ne laser (the wavelength λ = 632.8 nm) as light source. In DLS measurements, the intensity correlation function was measured at a temperature of 30 ^{o}C. The obtained intensity autocorrelation function, $G^{(2)}(t)$, is related to the electric field autocorrelation function, $g^{(1)}(t)$, by means of the Siegert relation. $g^{(1)}(t)$ is further related to the characteristic linewidth (Γ) distribution $G(\Gamma)$. Here, $G(\Gamma)$ can be calculated by a Laplace inversion of $g^{(1)}(t)$ using the CONTIN program. From the expression $\Gamma = D_{app} \cdot q^2$, the apparent translational diffusion coefficients (D_{app}) were determined. Γ is the decay rate, which is the inverse of the relaxation time (t). q is the scattering vector defined as $q = (4\pi n \sin(\theta/2)/\lambda)$ (where n is the refractive index of the solution, θ is the scattering angle, and λ is the wavelength of the incident laser light in vacuum). The apparent hydrodynamic radius ($R_{h,app.}$) can be determined by the Stokes-Einstein relationship $R_{h,app.} = k_B T/(6\pi\eta D_{app})$, where k_B, T, and η are the Boltzmann constant, the absolute temperature, and the solvent viscosity, respectively. Before the light scattering measurements, all sample solutions were filtered through a polytetrafluoroethylene filter with a pore size of 5 μm.

2 Characterization of PBLG-*b*-PEG-*b*-PBLG triblock copolymers

^{1}H NMR characterization

In this work, two kinds of triblock copolymers with different PBLG chain length were prepared through adjusting the amount of the initiator (NH_2-PEG-NH_2) during copolymer synthesis. Figure S1 show the ^{1}H NMR spectra (Avance 550, Bruker) of the copolymers using deuterated chloroform ($CDCl_3$) as solvent and tetramethylsilane (TMS) as an internal standard. The signal at δ = 3.6 ppm is ascribed to methyl protons (1,2) of the PEG block and the resonance signal of protons on methylene group of benzyl (5) of PBLG block occurs at δ = 5.1 ppm. The ratio of the integration of these two characteristic peak areas equals to the ratio of the methyl proton number of the PEG block to the methylene proton number of the benzyl of the PBLG block. Since the degree of polymerization (DP) of the PEG block is known (45), the numbers of the methylene protons on the PEG block and the benzyl of the PBLG block were respectively calculated and the DP of PBLG block was obtained. The repeating unit numbers of each PBLG chains of the two triblock copolymers were calculated to be 252 and 167, respectively (Table S1).

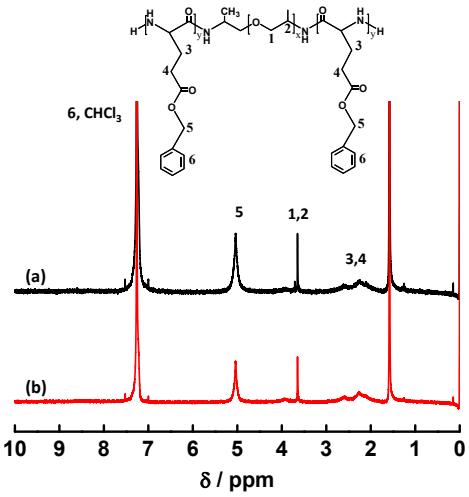

Figure S1. ^{1}H NMR spectra of $PBLG_{252}$-*b*-PEG_{45}-*b*-$PBLG_{252}$ (a) and $PBLG_{167}$-*b*-PEG_{45}-*b*-$PBLG_{167}$ (b) triblock copolymers in $CDCl_3$.

Gel permeation chromatography (GPC) characterization

The polydispersity index of PBLG-*b*-PEG-*b*-PBLG triblock copolymers was determined by gel permeation chromatography (GPC, Varian, PL GPC-50 plus). A 20 mM LiBr/DMF solution was used as the mobile phase at the flow rate of 0.8 mL/min (T = 49 °C). The calibration curve was obtained by narrow polydispersity PS standards. As shown in Figure S2, the GPC traces of the PBLG-*b*-PEG-*b*-PBLG copolymers display monomodal distributions, which indicate a well-controlled polymerization process. The PDI values of the copolymers are displayed in Table S1.

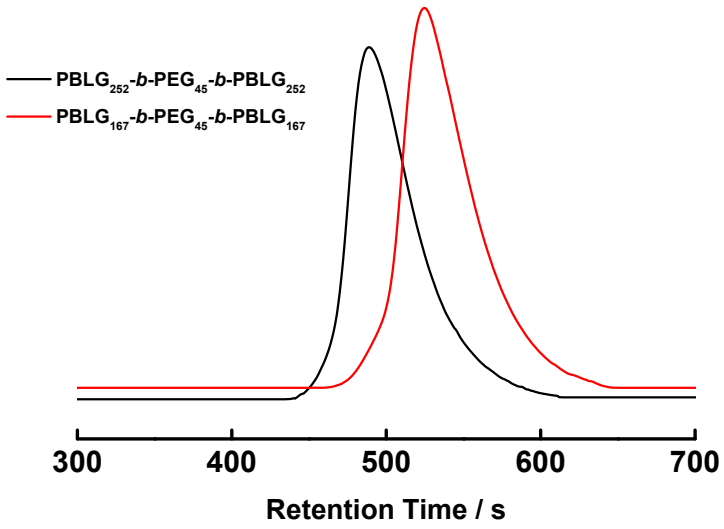

Figure S2. GPC traces of PBLG-*b*-PEG-*b*-PBLG triblock copolymers.

Table S1 Characteristics of PBLG-*b*-PEG-*b*-PBLG triblock copolymers

Sample	DP_{PBLG} [a]	M_n (g/mol) [b]	Polydispersity Index [c]
$PBLG_{252}$-*b*-PEG_{45}-*b*-$PBLG_{252}$	252	112,400	1.20
$PBLG_{167}$-*b*-PEG_{45}-*b*-$PBLG_{167}$	167	75,100	1.25

[a] Degree of polymerization of one PBLG segment determined by ^{1}H NMR.
[b] Number average molecular weight of BEB triblock copolymers, determined by ^{1}H NMR.
[c] Determined by GPC.

3 Characterization of the stability of the initial subunits

As shown in Scheme S1, the initial subunits were prepared in the first-step assembly through addition of water into the copolymer solution. The structure of the initial micellar subunits was frozen through adding a large amount of water. To examine the stability of the initial subunits, we characterized the variation of the apparent hydrodynamic radii ($R_{h,app}$) of the subunit I, II and III with time by DLS measurement. As shown in Figure S3, the $R_{h,app}$ of initial subunits remain almost unchanged with time, suggesting that the initial subunits are stable in aqueous solution. We have proved that after the addition of DMF, the micellar subunits aggregate into nanowire structure (Figure 1b in the main text). Therefore, the above results demonstrate that the subunits cannot aggregate in the aqueous solution unless they are "activated" upon the addition of DMF.

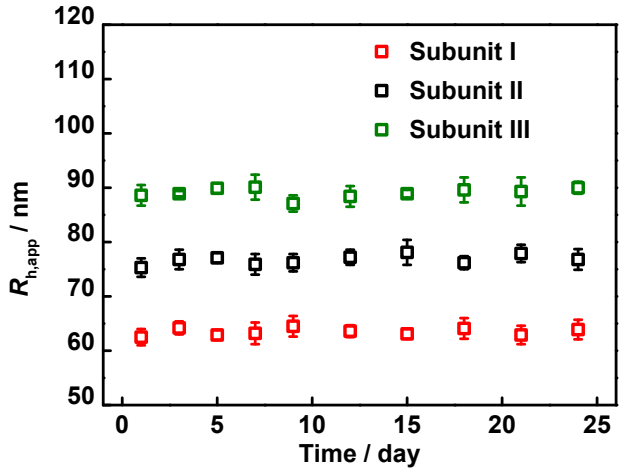

Figure S3. Plots of apparent hydrodynamic radius, $R_{h,app.}$ of aqueous initial subunit solutions without addition of DMF as a function of storing time.

4 Step-wise self-assembly of $PBLG_{167}$-*b*-PEG_{45}-*b*-$PBLG_{167}$ triblock copolymers

To examine the influence of the location of the structural defect on the defect-driven supramolecular polymerization, we used the micelles self-assembled from $PBLG_{167}$-*b*-PEG_{45}-*b*-$PBLG_{167}$ triblock copolymers as the polymerization subunits. The micellar subunits self-assembled from $PBLG_{167}$-*b*-PEG_{45}-*b*-$PBLG_{167}$ show nearly spherical morphologies (Figure S4a). As indicated by the red arrows in the inset, the structural defects are randomly distributed on the micellar subunits. This morphology can also be reproduced by the simulations. The triblock copolymers $\mathbf{R_8C_6R_8}$ with relatively shorter rod segment self-assemble into spherical micelles (Figure S4c). In these micelles, the rod blocks aggregate into the core in a radial manner and the coil blocks protrude outside to stabilize the spherical structure (Figure S4e). This chain arrangement manner results in the irregularly located structural defects on the micelles, conforming to the experimental results (Figure S4e). In the second-step assembly, these spherical micelles associate into agglomerates rather than in a well-ordered manner (Figure S4b, S4d). The irregular aggregation manner of these micelles (Figure S4f) is because of the randomly located structural defects.

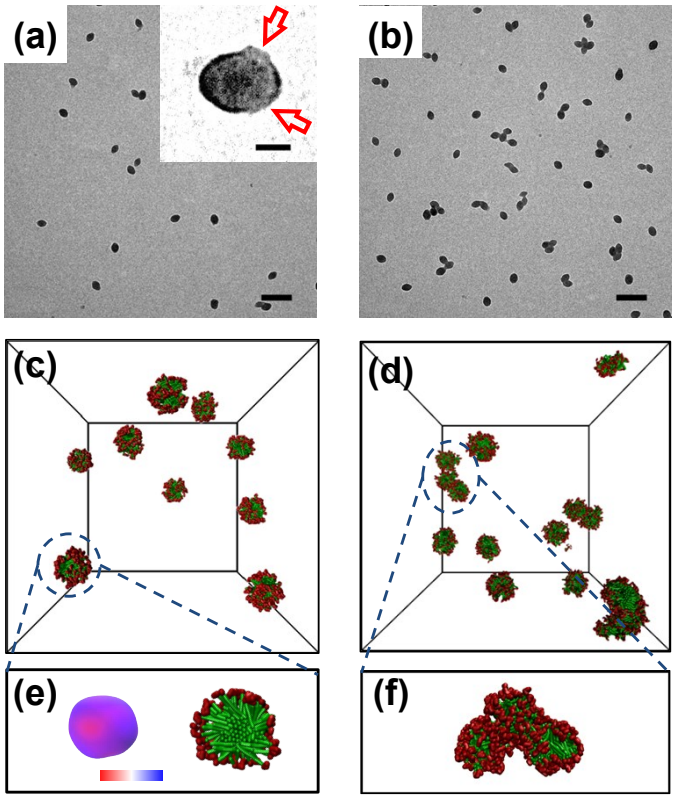

Figure S4. (a) TEM image of $PBLG_{167}$-*b*-PEG_{45}-*b*-$PBLG_{167}$ copolymer micelles with nearly spherical morphology. Inset is the image of the micelle after staining the sample with ruthenium tetroxide. The red arrows indicate the structural defects of the micelle. (b) TEM image of agglomerates self-assembled from spherical micellar subunits. (c) Simulation snapshots of spherical micelles self-assembled from $\mathbf{R_8C_6R_8}$ copolymers ($\varepsilon_{RR} = 3.5\varepsilon$, corresponding to the experimental condition after addition of water to the copolymer solution). (d) Simulation snapshots of agglomerates of spherical micelles self-assembled from $\mathbf{R_8C_6R_8}$ copolymers ($\varepsilon_{RR} = 5.0\varepsilon$, corresponding to the experimental condition in the second-step assembly). (e) The left image exhibits the density distribution of the coil segment on the micelle core. The color ranges from red (low-density region) to blue (high-density region). The right image is the cross-section of the micellar subunit. (f) Enlarged image of the agglomerates of the spherical micelles. Scale bar: 400 nm for (a,b); 50 nm for the insets of (a,b)

5 Cryo-TEM images of the hierarchical assemblies

The self-assembly of the various kinds of micellar subunits was examined by the cryo-TEM. Figure S5 shows the typical cryo-TEM images of the aggregates formed from the subunit I, II, III and the spherical subunit (self-assembled from $PBLG_{167}$-*b*-PEG_{45}-*b*-$PBLG_{167}$ copolymers). It can be found that the subunit I are connected in the end-to-end manner (Figure S5a). However, the subunit II and III can also connect in the end-to-side and side-to-side manners (Figure S5b and S5c). For the spherical subunit, the agglomerates without well-organized superstructures are formed (Figure S5d). These Cryo-TEM results are in good agreement with TEM testing (Figure 1b, Figure 4c,d in the main text and Figure S4b in the above text), indicating that the drying effects in the sample preparation can be ruled out.

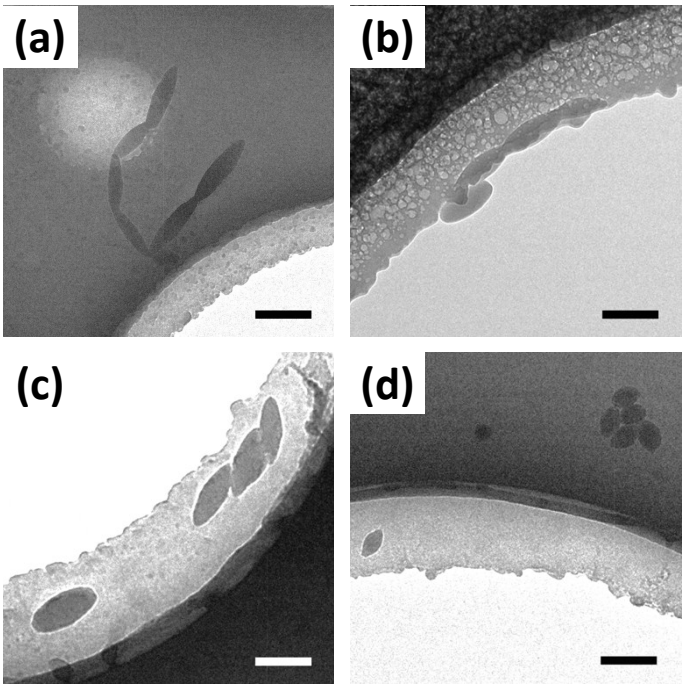

Figure S5. Cryo-TEM images of the aggregates self-assembled from different micellar subunits: (a) subunit I; (b) subunit II; (c) subunit III; (d) the spherical subunits which are self-assembled from $PBLG_{167}$-*b*-PEG_{45}-*b*-$PBLG_{167}$ copolymers. Scale bars: 200 nm.

6 Branching structures formed from the subunits

In the assembly, when the subunit occasionally connects with more than two subunits, the branching structures were observed. This connection is generated because the subunit possesses three reactive points (which is caused by the irregular distribution of the structural defects) or one reactive point on the subunit connects with two other reactive points (which results from the relatively larger exposed area of the structural defect than the other two structural defects). The typical branching structures are shown in Figure S6. The fraction of the branching structures increases from about 4.0% for the subunit I to 5.2% for the subunit II and 7.0% for the subunit III.

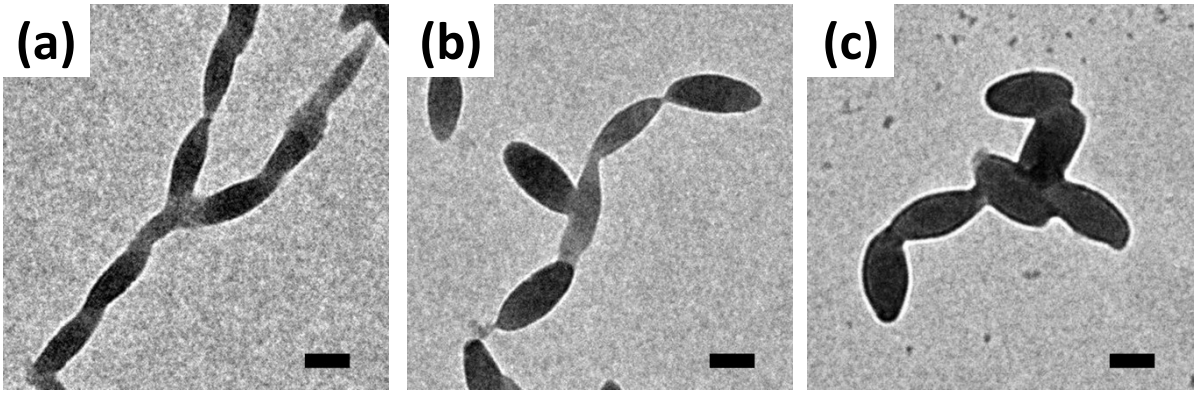

Figure S6. TEM images of the typical branching structures self-assembled from different micellar subunits: (a) subunit I; (b) subunit II; (c) subunit III. Scale bars: 100 nm.

7 Definitions and measurements of the parameters f_X, φ_c, p, X_n, and $Đ$

Number fraction f_X of the nanowire with degree of polymerization X

The parameter f_X characterizes the number fraction of the 1D assemblies with degree of polymerization X in the systems. The number fraction is given as

$$f_X = \frac{n_X}{\sum_X n_X} \qquad (S-1)$$

where n_X is the number of 1D assemblies with the degree of polymerization X. In the experiments, the parameter n_X was captured by mathematical statistics from the SEM images. By collecting more than 400 micelles and analyzing the images using Image-Pro Plus software, we obtained the number n_X of the 1D assemblies and then calculated f_X according to eq. (S-1).

The fraction of the supramolecular chains (φ_c)

The φ_c represents the number fraction of the supramolecular chains in an assembly system where the number of the micellar subunits is constant during the assembly.

$$\varphi_c = \frac{\sum_X n_X}{\sum_X X n_X} \qquad (S-2)$$

The extent of polymerization (p)

The parameter p characterizes the extent of polymerization and is given by

$$p = \frac{\sum_X (X-1) n_X}{\sum_X X n_X} \qquad (S-3)$$

Number-average degree of polymerization of the 1D assemblies (X_n)

The parameter X_n characterizes the number-average length of the 1D assemblies and is given by

$$X_n = \frac{\sum_X X n_X}{\sum_X n_X} \qquad (S-4)$$

Dispersity (*Đ*)

The parameter *Đ* was defined to characterize the size distribution of the 1D assemblies and is given by

$$Đ = \frac{\sum_{X} X^2 n_X \sum_{X} n_X}{\left(\sum_{X} X n_X\right)^2} \qquad (S-5)$$

8 Experimental observations of the time-dependent self-assembly

Time-dependent self-assembly of the subunits characterized by SEM

Time-dependent connection of micellar subunits was examined by SEM. Figure S7-S9 show the SEM images of the 1D assemblies self-assembled from the subunit I, II and III respectively with various self-assembly time (*t*). The subunit I, II and III are prepared at 50, 30 and 10 ^{o}C, respectively. As can be seen, with increasing *t*, the micellar subunits tend to connect with each other. In addition, at the same assembly time, the average length of the nanowires decreases from the subunit I to subunit II and III. The information provided by SEM images is consistent with the TEM observations (main text, Figure 2a-c, Figure 3g,h).

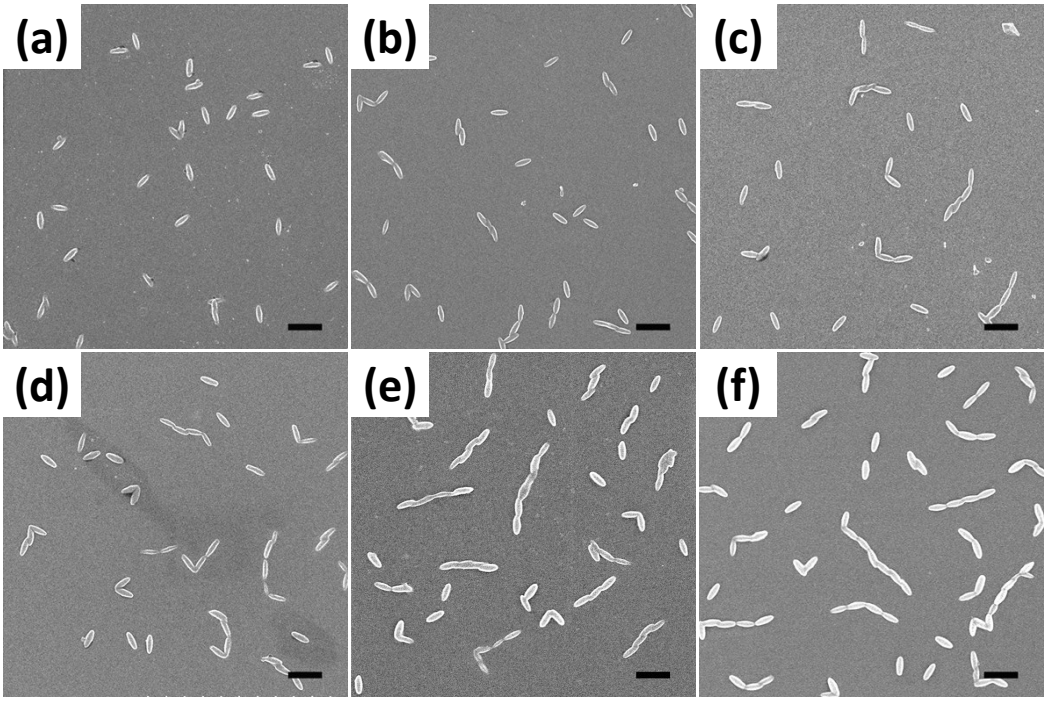

Figure S7 SEM images of the aggregates self-assembled from the subunit I with various self-assembly time (*t*): (a) 1 day, (b) 5 days, (c) 9 days, (d) 15 days, (e) 21 days, and (f) 24 days. Scale bars: 400 nm.

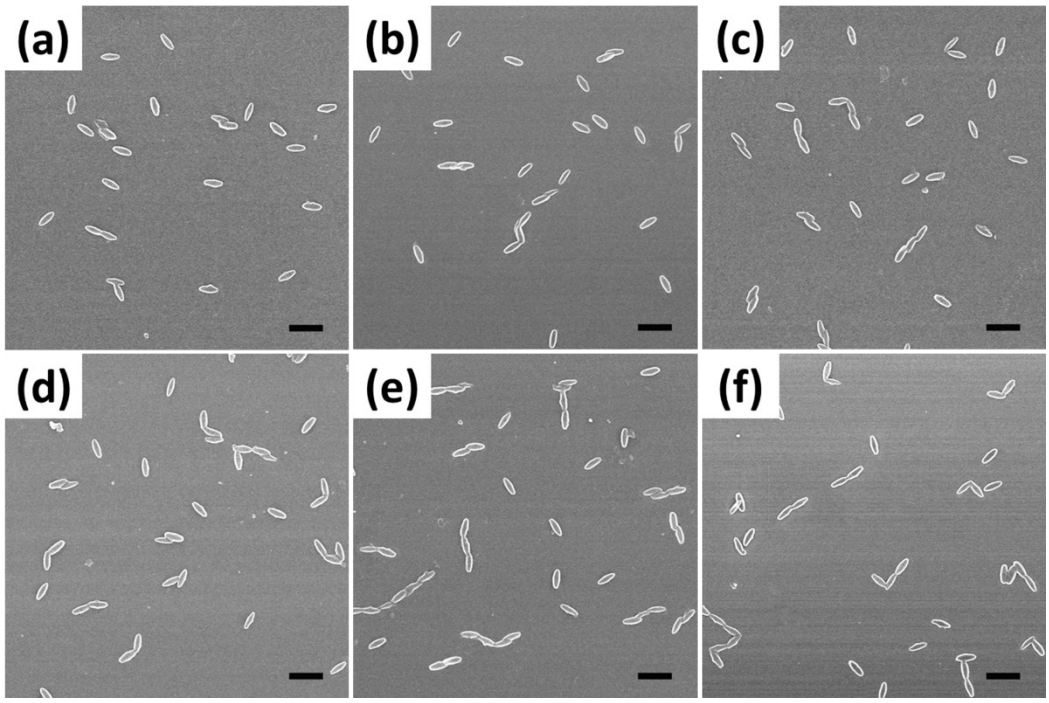

Figure S8 SEM images of the aggregates self-assembled from the subunit II with various self-assembly time (*t*): (a) 1 day, (b) 5 days, (c) 9 days, (d) 15 days, (e) 21 days, and (f) 24 days. Scale bars: 400 nm.

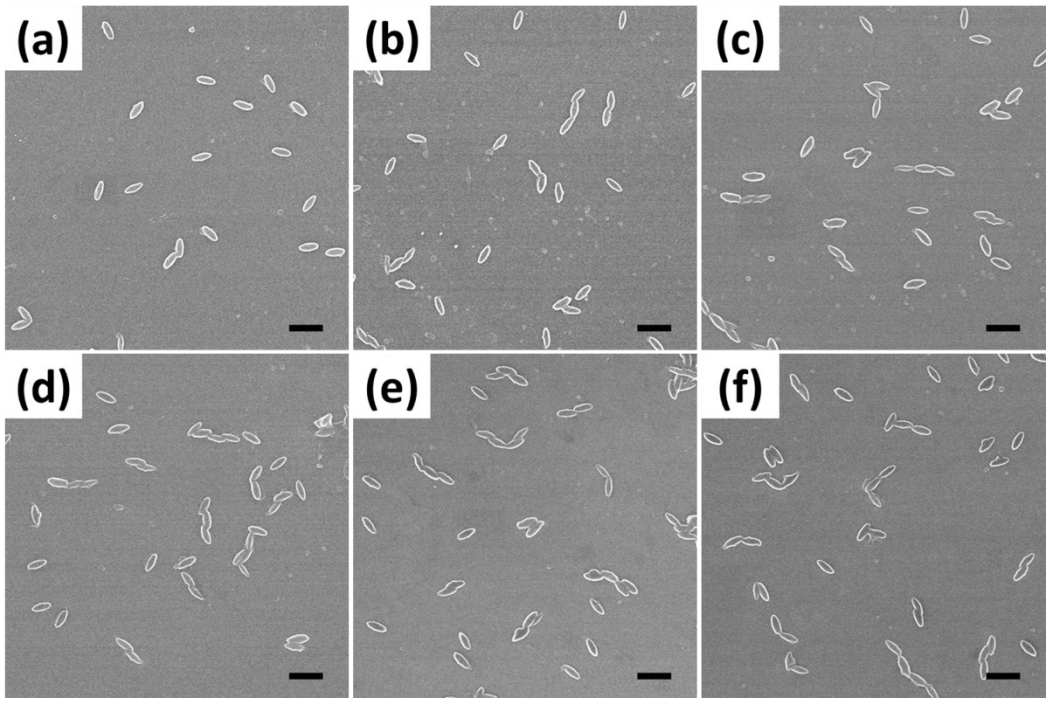

Figure S9 SEM images of the aggregates self-assembled from the subunit III with various self-assembly time (*t*): (a) 1 day, (b) 5 days, (c) 9 days, (d) 15 days, (e) 21 days, and (f) 24 days. Scale bars: 400 nm.

Number fraction of the nanowires with degree of polymerization *X*

Figure S10-S12 show the number fraction of the nanowires formed from various subunits against the degree of polymerization *X* at different assembling time. As can be seen, for the subunit I, the number fraction of micellar subunits joining in the polymerization gradually increases with time (from 0.15 to 0.65), indicating the progressive polymerization of the subunits (Figure S10). Here, *p* represents the extent of polymerization in step-growth polymerization. While for the subunit II and III, the increase of *p* with time becomes less obvious (Figure S11 and S12).

In addition, it was found that for all the subunits, f_X exhibits an exponential decay and the f_X data can be well fitted with the relationship $f_X = (1-p)p^{X-1}$ (a classical theoretical prediction of the number fraction distribution of polymers in the conventional step-growth polymerization).[S6] The results imply that the connection of subunits follows the step-by-step manner.

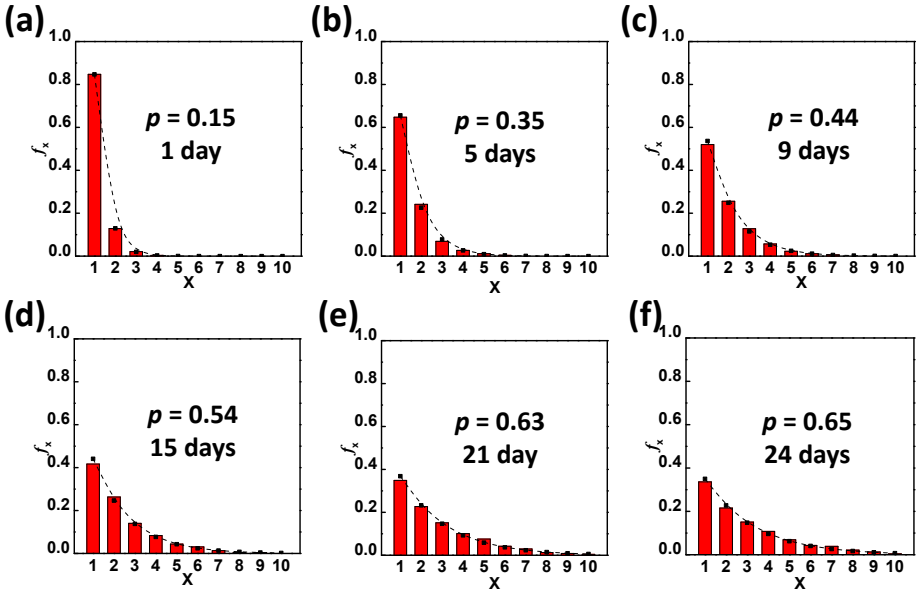

Figure S10 Number fraction, f_X, of the nanowires formed from the subunit I as a function of the degree of polymerization *X* at various assembly time: (a) 1 day, (b) 5 days, (c) 9 days, (d) 15 days, (e) 21 days, and (f) 24 days. The black dashed line is the theoretical number fraction, f_X, of the nanowires with *X* ($f_X=(1-p)p^{X-1}$).

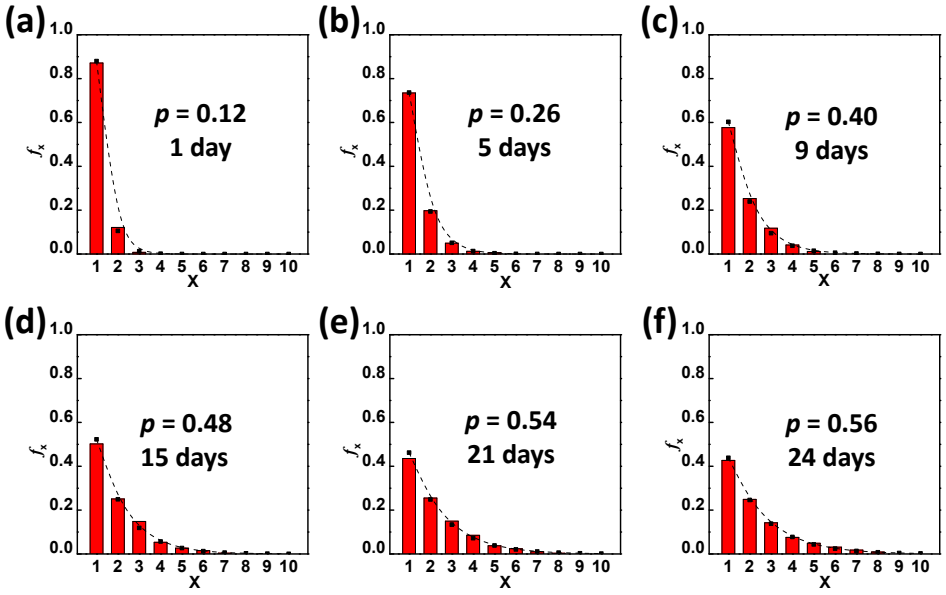

Figure S11 Number fraction, f_X, of the assemblies formed from the subunit II as a function of the degree of polymerization X at various assembly time: (a) 1 day, (b) 5 days, (c) 9 days, (d) 15 days, (e) 21 days, and (f) 24 days. The black dashed line is the theoretical number fraction, f_X, of the nanowires with X ($f_X=(1-p)p^{X-1}$).

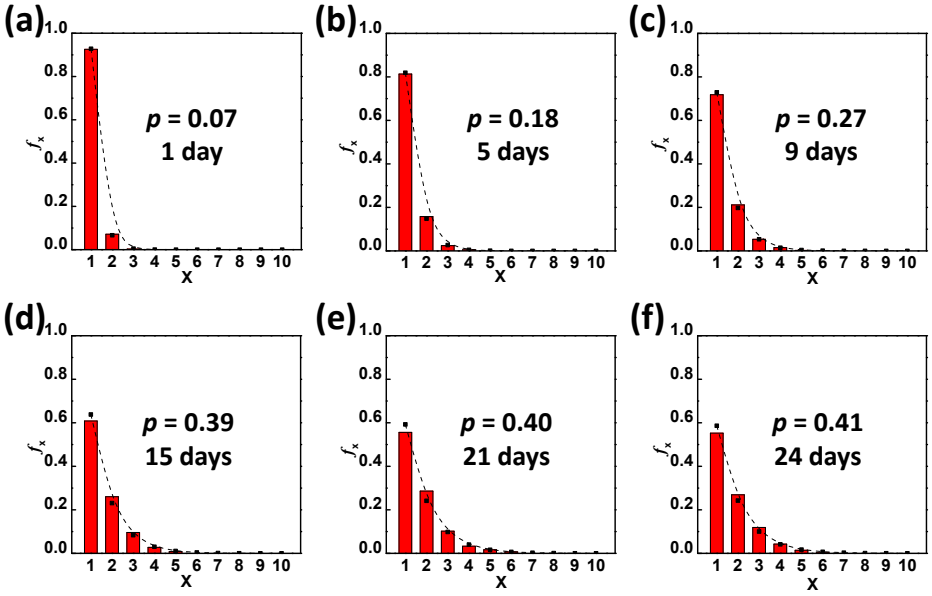

Figure S12 Number fraction, f_X, of the assemblies formed from the subunit III as a function of the degree of polymerization X at various assembly time: (a) 1 day, (b) 5 days, (c) 9 days, (d) 15 days, (e) 21 days, and (f) 24 days. The black dashed line is the theoretical number fraction, f_X, of the nanowires with X ($f_X=(1-p)p^{X-1}$).

9 A theoretical model of the supramolecular polymerization of micellar subunits

To quantitatively analyze the step-growth polymerization for the micellar subunits, we proposed a theoretical model of the supramolecular polymerization. In the derivation process, we adopt the mathematical method of the step-growth polymerization theory.[S7] Different from that in the classical step-growth polymerization, the two reactive points of the subunit in the model may possess different activities due to the fact that the two structural defects on the micellar subunit are not exactly the same. The supramolecular polymerization model was described in detail in this section.

We consider the polymerization of subunits in which the two reactive points with different activity are denoted by **A** and **B**. In the course of polymerization, a reactive point can react stochastically with both **A** and **B** reactive points. Therefore, there are three different types of reaction in this polymerization, which are reactions of **A**-to-**A**, **A**-to-**B** and **B**-to-**B**. We introduce a parameter α which defines the ratio of activity between **A** and **B** reactive points.

The relationship between X_n and t

The assembly rate constant between reactive points **A** is set as k. Thus, the assembly rate constant between reactive points **A** and **B** is $\frac{k}{\alpha}$ and that between reactive points **B** is $\frac{k}{\alpha^2}$. Based on the kinetic theory of the step-growth polymerization, the following relationships hold for this system:

$$\frac{d[A]}{dt} = k[A]^2 + \frac{k}{\alpha}[A][B] \qquad (S-6)$$

$$\frac{d[B]}{dt} = \frac{k}{\alpha}[A][B] + \frac{k}{\alpha^2}[B]^2 \qquad (S-7)$$

[A] and [B] are the concentration of **A** and **B** reactive points at the given time *t*. By combining Eq. (S-6) and Eq. (S-7) together, we can obtain:

$$\frac{d([A]+[B])}{dt} = \frac{d[A]}{dt} + \frac{d[B]}{dt} = k[A]^2 + \frac{2k}{\alpha}[A][B] + \frac{k}{\alpha^2}[B]^2 = k([A] + \frac{1}{\alpha}[B])^2 \qquad (S-8)$$

At the beginning of polymerization, the concentration of all subunits is set as C_0. The initial concentrations of reactive point **A** and **B** are as follows:

$$[A]_0 = [B]_0 = C_o \qquad (S-9)$$

According to the definition of the extent of polymerization p

$$p = \frac{2C_0 - [A] - [B]}{2C_0} \qquad (S-10)$$

The contributions of the three reaction types, A-to-A, A-to-B, and B-to-B to the extent of polymerization p are $\frac{\alpha^2}{(\alpha+1)^2}$, $\frac{2\alpha}{(\alpha+1)^2}$ and $\frac{1}{(\alpha+1)^2}$, respectively. The extents of polymerization for A and B reaction points were respectively written as

$$p_A = \frac{2\alpha}{\alpha+1}p \qquad (S-11)$$

$$p_B = \frac{2}{\alpha+1}p \qquad (S-12)$$

Noted that, these relationships are only applicable to the initial stage of polymerization, where neither reactive point A nor reactive point B is totally consumed. In other words, the following relationships should be satisfied: $0 < p_A < 1$ and $0 < p_B < 1$. Therefore, the valid range of values of p can be obtained: $0 < p < \frac{\alpha+1}{2\alpha}$.

Therefore, the relationship between [A] and [B] is as follows:

$$\frac{C_0 - [A]}{C_0 - [B]} = \frac{\frac{2\alpha^2}{(\alpha+1)^2}p + \frac{2\alpha}{(\alpha+1)^2}p}{\frac{2\alpha}{(\alpha+1)^2}p + \frac{2}{(\alpha+1)^2}p} = \alpha \qquad (S-13)$$

According to Eq. (S-13), the concentrations of A and B reactive points follow the formulas below:

$$[A] = \frac{\alpha}{\alpha+1}([A]+[B]) - \frac{\alpha-1}{\alpha+1}C_0 \qquad (S-14)$$

$$[B] = \frac{1}{\alpha+1}([A]+[B]) + \frac{\alpha-1}{\alpha+1}C_0 \qquad (S-15)$$

With combing Eq. (S-8), Eq. (S-14) and Eq. (S-15), the following relationship can be obtained:

$$\frac{d([A]+[B])}{dt}=\frac{k[(\alpha^2+1)([A]+[B])-(\alpha-1)^2C_0]^2}{\alpha^2(\alpha+1)^2} \qquad (S-16)$$

With integrating Eq. (S-16), the following equation can be obtained:

$$[A]+[B]=\frac{[(\alpha-1)^2kC_0t+2\alpha^2]C_0}{(\alpha^2+1)kC_0t+\alpha^2} \qquad (S-17)$$

In the step-growth polymerization, the expression of X_n can be derived from its definition:

$$X_n=\frac{[A]_0+[B]_0}{[A]+[B]}=\frac{2C_0}{[A]+[B]} \qquad (S-18)$$

With Combining the Eq. (S-17) and Eq. (S-18), the relationship between X_n and t can be obtained:

$$X_n=\frac{2(\alpha^2+1)kC_0t+2\alpha^2}{(\alpha-1)^2kC_0t+2\alpha^2} \qquad (S-19)$$

When $\alpha=1.0$ (implying the activities of the two reactive points are identical), Eq. (S-19) becomes $X_n=2kC_0t+1$, which is reverted to the classical formula of X_n in the conventional step-growth polymerization. We used Eq. (S-19) to fit the data of X_n as a function of t in the experiments (Figure 2e, Figure 5a,b).

The relationship between *Đ* and X_n

The relationship between *Đ* and X_n was obtained via adopting the method developed by Macosko and Miller.[S8,S9] The total number of subunits in the initial system is set as *N*, and the subunit mass is *M*. Picking the subunits in the middle of a random chain, we denoted the expected mass of chains which contain a randomly selected **A** or **B** ends as w_A or w_B, and introduced four variables w_A^i, w_A^o, w_B^i, and w_B^o. Here w_A^i represents the expected mass attached to the reactive point **A** via looking inward (toward the reactive point **B**) from this reactive point **A** and w_A^o represents the expected mass attached via looking outward from the reactive point **A**. Similarly, w_B^i and w_B^o represent the expected inward

and outward mass attached to the reactive point **B** in this subunits, respectively. The following relationships hold for this system

$$w_A = w_A^i + w_A^o \qquad (S-20)$$

$$w_B = w_B^i + w_B^o \qquad (S-21)$$

$$w_A^i = M + w_B^o \qquad (S-22)$$

$$w_A^o = p_A\left(\frac{\alpha}{\alpha+1}\cdot w_A^i + \frac{1}{\alpha+1}\cdot w_B^i\right) \qquad (S-23)$$

$$w_B^i = M + w_A^o \qquad (S-24)$$

$$w_B^o = p_B\left(\frac{\alpha}{\alpha+1}\cdot w_A^i + \frac{1}{\alpha+1}\cdot w_B^i\right) \qquad (S-25)$$

Eq. (S-22) and Eq. (S-23) state the inward and outward masses attached to reactive point **A**. Similarly, Eq. (S-24) and Eq. (S-25) express the inward and outward masses of reactive point **B**. Being analogous to calculation of the weight-average molecular weight in molecular polymerization, we can solve these equations and obtain the weight-average nanowire weight

$$M_W = \frac{w_A}{2} + \frac{w_B}{2} = \frac{M\left[(2\alpha^2+2)p + (\alpha+1)^2\right]}{(\alpha+1)^2 - 4\alpha p} \qquad (S-26)$$

The number-average nanowire weight, obtained from the extent of polymerization p, are given by

$$M_n = \frac{N\cdot M}{(1-p)N} = \frac{M}{1-p} \qquad (S-27)$$

Combining the Eq. (S-26) and Eq. (S-27), we can obtain the dispersity as

$$Đ = \frac{M_W}{M_n} = \frac{\left[(2\alpha^2+2)p + (\alpha+1)^2\right](1-p)}{(\alpha+1)^2 - 4\alpha p} \qquad (S-28)$$

Additionally, we can replace p in Eq. (S-28) with the equation $p = 1 - \frac{1}{X_n}$ and obtain

$$Đ = \frac{(3\alpha^2+2\alpha+3)X_n - 2\alpha^2 - 2}{(\alpha-1)^2 X_{\mathrm{n}}^2 + 4\alpha X_{\mathrm{n}}} \qquad (S-29)$$

Hence, the relationship between $Đ$ and X_{n} is associated with parameter α. When $\alpha = 1.0$, Eq. (S-

29) becomes $Đ = 2 - \frac{1}{X_n}$, which is reverted to the classical formula of *Đ* in the conventional step-growth polymerization. Noted that, these theoretical equations are only applicable to the initial stage of polymerization where the p and X_n are in the following range: $0 < p < \frac{\alpha + 1}{2\alpha}$, and $X_n < \frac{2\alpha}{\alpha - 1}$. We used Eq. (S-29) to fit the data of *Đ* as a function of X_n in experiments (Figure 2f, Figure 5d,e).

10 Estimation of the subunit concentration C_{sub}

To obtain the assembly rate constant k of the micellar subunits, the initial concentration of subunits (C_0) in the experiments should be firstly estimated. Taking the subunit I as an example, in the 5.0 mL initial solution of $PBLG_{252}$-*b*-PEG_{45}-*b*-$PBLG_{252}$ copolymer (M_w=146100 g/mol), the mass concentration of polymer was 0.25 g/L. Therefore, the number of polymer chains in the initial polymer solution was

$$N_{polymer} = 0.25\text{g/L} \times 0.005\text{L} \div 134900\text{g/mol} = 9.27\times10^{-9}\,\text{mol}$$

which was unchanged during the step-wise self-assembly. The addition of 1.0 mL water into the initial polymer solution triggered the assembly of polymers into the micelles.

The weight-average molecular weight of the micelles (M_w^{sub}) was obtained from static light scattering (SLS) measurements. In static LLS, the angular dependence of the excess absolute time-average scattered intensity, *i.e.* Rayleigh ratio R of the dilute polymer solutions was measured. R is related to the weight-averagemolarmass (M_w), polymer concentration (C), and the scattering angle (θ) as

$$\frac{KC}{R(\theta,C)} = \frac{1}{M_w}\left(1 + \frac{R_g^2 q^2}{3}\right) + 2A_2C$$

where $K = 4\pi^2 n^2 (\mathrm{d}n/\mathrm{d}C)^2/(N_A\lambda^4)$ and $q = 4\pi n\sin(\theta/2)/\lambda$ with N_A, $\mathrm{d}n/\mathrm{d}C$, n, and λ being the Avogadro number, the specific refractive index increment, the solvent refractive index, and the wavelength of the light in vacuum, respectively, A_2 is the second virial coefficient, and R_g is the z-average radius of gyration of the aggregates in solution. By extrapolating to zero concentration and zero angle, M_w^{sub} value of the micelles can be calculated. Figure S13 is a typical Zimm plot of subunit I.

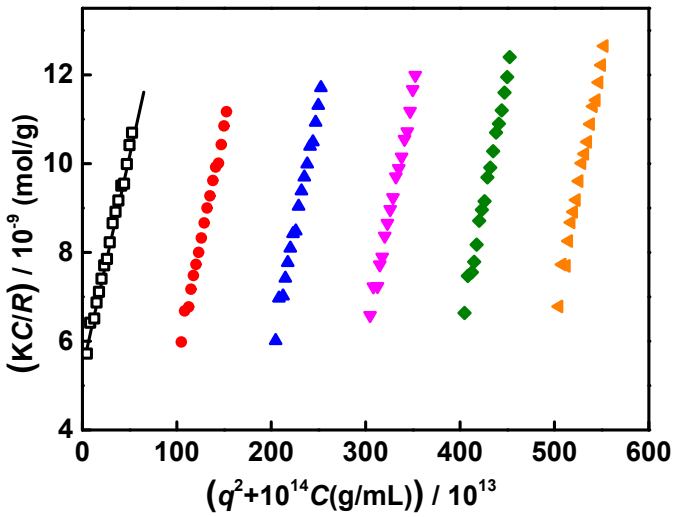

Figure S13 Typical Zimm plot of subunit I. The black squares represent the extrapolated data to zero concentration.

According to Figure S13, the weight-average molecular weight of the subunit I was calculated to be M_w^{sub} = 1.86×10^{8}g/mol. Therefore, the number of subunits in the course of supramolecular polymerization was

$$N_{sub} = 9.27\times10^{-9}\ \text{mol} \div (1.86\times10^{8}\ \text{g/mol} \div 134900\ \text{g/mol}) = 6.72\times10^{-12}\ \text{mol}$$

After dialysis and the addition of DMF, the volume of the solution was 6.25 mL. As a result, the molar concentration of the subunit I was

$$C_0 = 6.72\times10^{-12}\ \text{mol} \div 0.0065\text{L} = 1.03\times10^{-9}\ \text{mol/L}$$

Based on the above methods, the molar concentration of all the subunits C_0 can be estimated from the weight-average molecular-weight of copolymers (M_w) and that of micelles (M_w^{sub}). The detailed results of estimation is shown in Table S2.

Table S2 Laser light scattering characterization of the initial micelles

Sample	M_w (g/mol) [a]	M_w^{sub} (g/mol) [b]	C_0 (mol/L) [c]
Subunit I	134,900	1.86×10^{8}	1.03×10^{-9}
Subunit II	134,900	2.08×10^{8}	9.25×10^{-10}
Subunit III	134,900	2.23×10^{8}	8.63×10^{-10}

[a] Weight-average molecular-weight of $PBLG_{252}$-*b*-PEG_{45}-*b*-$PBLG_{252}$ copolymers, calculated from the number-average molecular-weight and polydispersity index of copolymers in Table S1.

[b] Weight-average molecular-weight of subunits, which was determined by SLS measurements.

[c] Molar concentration of subunits in the course of polymerization.

11. Influence of copolymer composition on the supramolecular polymerization

To examine the influence of copolymer composition on the supramolecular polymerization, we synthesized triblock copolymers with different lengths of PBLG blocks, which are $PBLG_{206}$-*b*-PEG_{45}-*b*-$PBLG_{206}$, $PBLG_{167}$-*b*-PEG_{45}-b-$PBLG_{167}$ and $PBLG_{108}$-*b*-PEG_{45}-*b*-$PBLG_{108}$. Figure S14a-c show the images of the micellar subunits self-assembled from the above copolymers. As can be seen, with decreasing the length of PBLG, the morphologies of the subunits change from short rods to spheres. In the corresponding second assembly step, the rod-like micellar subunits of $PBLG_{206}$-*b*-PEG_{45}-*b*-$PBLG_{206}$ self-assemble into one-dimensional hierarchical structures (shown in Figure S14d). These one-dimensional structures are shorter and less regular than the nanowires formed from $PBLG_{252}$-*b*-PEG_{45}-*b*-$PBLG_{252}$ (Figure 1b in the main text). For the micellar subunits of $PBLG_{167}$-*b*-PEG_{45}-*b*-$PBLG_{167}$ and $PBLG_{108}$-*b*-PEG_{45}-*b*-$PBLG_{108}$, the aggregation of the subunits is more irregular and few one-dimensional structures can be found (Figure S14e,f).

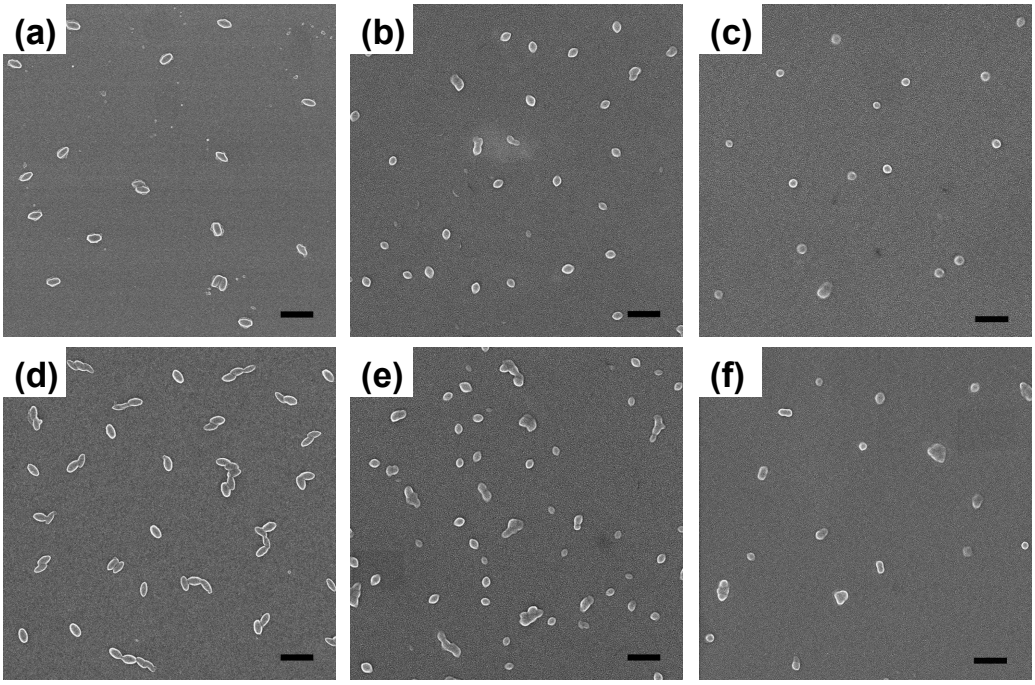

Figure S14. (a-c) The micellar subunits self-assembled from PBLG-*b*-PEG-*b*-PBLG with different PBLG length: (a) $PBLG_{206}$-*b*-PEG_{45}-*b*-$PBLG_{206}$; (b) $PBLG_{167}$-*b*-PEG_{45}-*b*-$PBLG_{167}$; (c) $PBLG_{108}$-*b*-PEG_{45}-*b*-$PBLG_{108}$. (d-f) The aggregates self-assembled from these micellar subunits: (d) subunits of $PBLG_{206}$-*b*-PEG_{45}-*b*-$PBLG_{206}$; (e) subunits of $PBLG_{167}$-*b*-PEG_{45}-*b*-$PBLG_{167}$; (f) subunits of $PBLG_{108}$-*b*-PEG_{45}-*b*-$PBLG_{108}$. Scale bars: 400 nm.

12 Brownian dynamics (BD) simulation method

BD is a coarse-grained mesoscopic simulation method.[S10,S11] In the simulation, each bead represents a cluster of atoms and is connected by the bond stretching potential. Here, due to the rigid α-helix conformation of PBLG, the PBLG-*b*-PEG-*b*-PBLG triblock copolymer can be regarded as rod-coil-rod triblock copolymer model. We constructed a coarse-grained model with two rigid segments and one coil segment. As shown in Figure 1d, $PBLG_{167}$-*b*-PEG_{45}-*b*-$PBLG_{167}$ copolymer was modeled as $\mathbf{R_8C_6R_8}$, the green beads **R** and red beads **C** denote the PBLG block and PEG block, respectively. The rigidity of rod blocks and the pairwise interaction are given by the angle bend potential and the Lennard-Jones potential, respectively. The time evolution of the beads obeys the Langevin equation. The details regarding the choice of bead number and interaction parameters can be referred to Section 13 in the following text. For both the rod and coil blocks, the neighboring beads are connected by a bond modelling by a harmonic spring potential, given by

$$U_{bond}(r) = \frac{1}{2}k_b(r - r_0)^2 \qquad (S-30)$$

where k_b is the bond spring constant, r is the distance between the chemically bonded beads, and r_0 is the equilibrium bond length.

To model the rigidity of rod blocks, an angle bending potential $U_{angle}(\theta)$ is introduced

$$U_{angle}(\theta) = \frac{1}{2}k_a(\theta - \theta_0)^2 \qquad (S-31)$$

where k_a is the angle spring constant, θ is the angle between two neighboring bonds, and θ_0 is the equilibrium angle. The interaction between any pair of beads is given by the standard Lennard-Jones (LJ) potential U_{ij}

$$U_{ij} = \begin{cases} 4\varepsilon_{ij}\left[\left(\frac{\sigma_{ij}}{r_{ij}}\right)^{12} - \left(\frac{\sigma_{ij}}{r_{ij}}\right)^{6} - \left(\frac{\sigma_{ij}}{r_{ij}^c}\right)^{12} + \left(\frac{\sigma_{ij}}{r_{ij}^c}\right)^{6}\right], & r \le r_{ij}^c \\ 0, & r > r_{ij}^c \end{cases} \qquad (S-32)$$

where $r_{ij} = \left| \vec{r}_i - \vec{r}_j \right|$, with $\vec{r}_i$ and $\vec{r}_j$ being the location of the *i*-th and *j*-th beads, respectively. r_{ij}^c and ε_{ij} are the cutoff distance and the interaction parameter between beads *i* and *j*, respectively. The amphiphilicity of polymer blocks in this model is realized by introducing different cutoff distances of LJ potential and the interaction parameter, which was given in the next section. The effect of solvent molecules is implicitly treated by a noise term, which satisfies a fluctuation-dissipation relation.

All the simulation are carried out on a 100 × 100 × 100 cubic cell using a Brownian Dynamic algorithm with the temperature controlling method (NVT ensemble).[S10,S12] The simulation snapshots for the subunit I, II and III are shown in Figure S15. The simulations were performed by applying the simulator, coarse grained molecular dynamics program based on LAMMPS.[S13] Other BD simulation conditions were provided in the Section 13 in the following text.

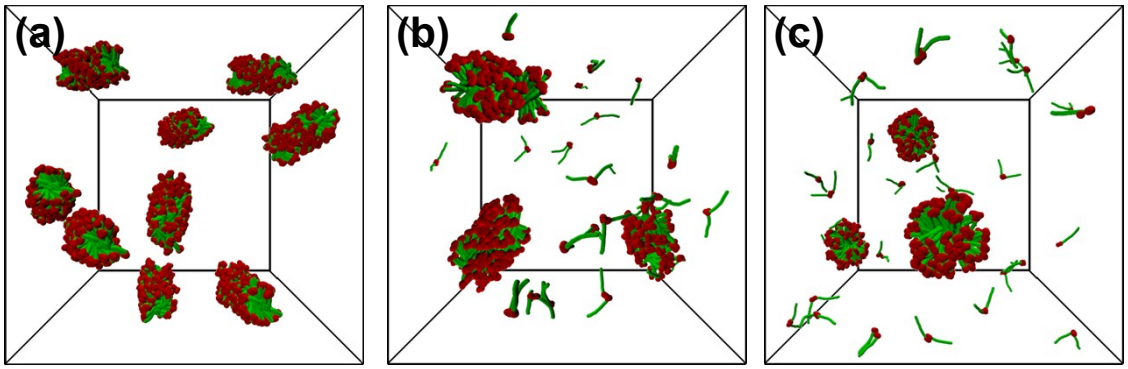

Figure S15. Simulation snapshots of micelles self-assembled from $\mathbf{R_{12}C_6R_{12}}$ at different interaction parameters: (a) ε_{RR} = 3.5ε (Corresponds to the subunit I). (b) ε_{RR} = 3.2ε (Corresponds to the subunit II). (c) ε_{RR} = 2.6ε (Corresponds to the subunit III).

13 Parameter settings in the simulations

To capture the essential feature of the experimental systems, we set the important parameters close to those of the experiment systems. The choices of important parameters are discussed and explained as follows.

Bead numbers

The bead numbers in rod and coil blocks were chosen appropriately so that their relative length matches the experimental data. Taking $PBLG_{252}$-*b*-PEG_{45}-*b*-$PBLG_{252}$ triblock copolymer as an example, the degrees of polymerization for PBLG block and each PEG grafted chain are $N_{PBLG} = 252$ and $N_{PEG} = 45$. Since 3.6 BLG form a 0.54 nm structure unit and 1 EG occupies 0.35 nm,[S14] the average length ratio of rigid PBLG to ideal PEG chain is $(N_{PBLG} \times 0.54/3.6):(N_{PEG} \times 0.35) \approx 2.4$. Firstly, the bead number for the middle coil block ($N_C = 6$) was chosen. To match the experiments, the average length ratio of **R** rod block to **C** coil block should satisfy the relation $(N_R \times 1.0):(N_C \times 1.0) = 2.4$, where N_R is the bead number in **R** rod block and 1.0 is the bond length. Thus, the bead number of **R** rigid segment was calculated to be 12, and then $PBLG_{252}$-*b*-PEG_{45}-*b*-$PBLG_{252}$ triblock copolymer was modeled as $\mathbf{R_{12}C_6R_{12}}$.

Bonds and Angles

The PEG segment is flexible, and thus only a harmonic spring force was applied for the coil chains. Since the PBLG with α-helix conformation can be considered as a rigid molecule, in the simulation, the angle force was employed to guarantee the rigidity of the backbone, by setting the angle constant $k_a = 100\varepsilon$ and θ_0=180°.[S10-S12,S14,S15] The value of k_b is set to be 100 ε/σ^2 to avoid the over-stretching of bonds. The equilibrium bond length r_0 is 1.0σ, where ε and σ are the units of energy and length, respectively.

Cut-off radius

Taking account of the solvent selectivity, the cut-off distance rules of the LJ potential for blocks in poor and good solvents are defined as follows. If the blocks are hydrophilic, the beads could not aggregate in the solution, the cut-off distance r^c was set to be $2^{1/6}\sigma$, corresponding to a purely repulsive interaction between the beads.[S10-S12] If the blocks are hydrophobic, the beads could aggregate, the cut-off distance r^c was set to be 2.5σ, corresponding to the short-range attractive interaction between the beads.[S15] In addition, a purely repulsive interaction was adopted for incompatible blocks, by setting $r^c = 2^{1/6}\sigma$.[S10-S12] In this work, for the hydrophilic **C** coil blocks, the **C-C** beads are effectively repelled by each other by setting r_{CC}^c as $2^{1/6}\sigma$. For the hydrophobic **R** rod blocks, the **R-R** beads are effectively attracted by each other and the behavior is modeled by setting r_{RR}^c to be 2.5σ. To mimic the immiscibility between hydrophilic and hydrophobic blocks, r_{RC}^c were set as $2^{1/6}\sigma$.[S10-S12]

Interaction parameters in the first-step self-assembly

In the experiments, the processes of adding water can lead to the change of solution environment and the aggregation of triblock copolymers. During the simulation, the assembly of copolymer is realized by setting different pairwise interaction parameters ε_{ij} as follows. The interactions between **R** and **R** blocks (**R-R** interaction) were modeled with an attractive potential to describe the hydrophobicity of PBLG blocks. The **C-C** and **R-C** interactions were modeled with purely repulsive potential, corresponding to hydrophilic nature of PEG blocks and the incompatibility between two blocks, respectively. The stronger hydrophobicity was realized by increasing the interaction strength ε_{RR} between **R** and **R** beads. For the pair of **C-C** beads and **R-C** beads with repulsive interactions, the interaction parameters ε_{ij} were set as $\varepsilon_{CC} = \varepsilon_{RC} = 1.0\varepsilon$, where ε is the unit of energy. The interaction

parameters ε_{RR} were set to be 3.5ε, 3.2ε and 2.6ε, corresponding to the micellization conditions at 50, 30 and 10 ^{o}C, respectively.[S10-S12,S14,S15]

Interaction parameters in the second-step self-assembly

In the second-step assembly, the micelles swell after the addition of DMF, causing more exposure of PBLG chains to the solvent. As a result, the solvophobic interaction at the micelle ends increases. To simulate this situation, we increased the interaction parameter ε_{RR} to 5.0ε. In addition, the molecular exchange between micelles was hindered. To simulate this state, we fixed the cores of the micelles in the second-step assembly.

Simulation time

In the simulation of the first-step self-assembly, 1.0×10^6 BD steps (5000τ) were carried out so that the computing time is long enough for the system to achieve an equilibrium state. In the simulation of the second-step self-assembly, 5.0×10^6 BD steps (25000τ) were carried out. The computing time is long enough for the systems to achieve the equilibrium.

Density distribution of coil segments on the micelle core

For the micelles assembled from the triblock copolymers, the rod blocks aggregate to form the micelle cores and the coil blocks distribute in the corona to stabilize the micelle. The order packing of rod blocks influences the distribution of coil blocks, causing imperfect coverage of coil blocks on some area of the micelle core. To describe the distribution of the coil segments for various kinds of subunits, we calculated the density of coil segments D_{coil} at different locations on the micelle core. Here, the density of coil segments D_{coil} was defined as the amount of the **C** beads wrapping each **R** bead. The 3D distribution of the coil segment density was then obtained by coloring the **R** beads with different colors according to the D_{coil} values (Figure 1f, Figure 3d and f). In the images, the red regions

are the **R** beads that are not covered by the hydrophilic coil segments. Those regions can be considered as the structural defects on the micellar subunits.

References

S1. D. S. Poché, M. J. Moore and J. L. Bowles, *Synth. Commun*., **1999**, *29*, 843.

S2. E. R. Blout and R. H. J. Karlson, *J. Am. Chem. Soc.,* **1956**, *78*, 941.

S3. T. J. Deming, *Adv. Polym. Sci*., **2006**, *202*, 1.

S4. C. Yang, Q. Li, C. Cai and J. Lin, *Langmuir*, **2016**, *32*, 6917.

S5. Z. Zhuang, C. Cai, T. Jiang, J. Lin and C. Yang, *Polymer*, **2014**, *55*, 602.

S6. G. Odian, *Principles of polymerization*, Wiley, New York, 4th edn., 2004.

S7. W. F. Reed, A. M. Alb, *Monitoring Polymerization Reactions: From Fundamentals to Applications*, Wiley, 1st edn., 2014.

S8. C. W. Macosko and D. R. Miller, *Macromolecules*, **1976**, *9*, 199.

S9. E. Ozizmir and G. Odian, *J Polym. Sci. Polym. Chem.*, **1980**, *18*, 2281.

S10. G. S. Grest and K. Kremer, *Phys. Rev. A*, **1986**, *33*, 3628.

S11. G. K. Bourov and A. Bhattacharya, *J. Chem. Phys.*, **2003**, *119*, 9219.

S12. Q. Zhang, J. Lin, L. Wang and Z. Xu, *Prog. Polym. Sci.*, **2017**, *75*, 1.

S13. Lammps. http://lammps.sandia.gov.

S14. C. Cai, Y. Li, J. Lin, L. Wang, S. Lin, X.-S. Wang and T. Jiang, *Angew. Chem. Int. Ed.* **2013**, *52*, 7732.

S15. Z. Guan, L. Wang and J. Lin, *Biomacromolecules*, **2017**, *18*, 797.